

All-fiber saturable absorber based on nonlinear multimode interference with enhanced modulation depth

TENG WANG^{1,2,3,*}, YONGMIN JUNG^{1,4}, PETER HORAK¹, XIANGLONG ZENG², AND DAVID J. RICHARDSON¹

¹Optoelectronics Research Centre, University of Southampton, Southampton SO17 1BJ, UK

²Key Laboratory of Specialty Fiber Optics and Optical Access Networks, Shanghai University, Shanghai 200444, China

³College of Computer and Information Engineering, Shanghai Polytechnic University, Shanghai 201209, China

⁴e-mail: ymj@orc.soton.ac.uk

*Corresponding author: tengwang@shu.edu.cn

Compiled September 1, 2021

We experimentally demonstrate a passively mode-locked fiber ring laser using a small-core fiber – graded index multimode fiber – single mode fiber (SCF-GIMMF-SMF) structure as an effective saturable absorber (SA) based on nonlinear multimode interference (NL-MMI) effect. A small-core fiber is used as an input single mode fiber to improve coupling of power into higher-order modes in a multimode fiber and to enhance the modulation depth of the structure. Stable fundamental mode-locked operation is obtained at a pump threshold of 166 mW and the output soliton pulses have 647 fs duration at 1557.96 nm with a 5.2 nm spectral width at a repetition rate of 19.37 MHz. This NL-MMI SA can be applied to high-power mode-locked fiber lasers owing to its inherent high damage threshold, compact size, wavelength independent operation and fabrication simplicity. © 2021 Optical Society of America

<http://dx.doi.org/10.1364/ao.XX.XXXXXX>

1. INTRODUCTION

Mode-locked fiber lasers (MLFLs) have developed rapidly over the last two decades and are widely used to generate ultrashort pulses in the picosecond to femtosecond region because of their unique advantages of high peak power, excellent beam quality, compact structure, high efficiency and reliability [1]. A saturable absorber (SA) is one of the key components of efficient MLFLs and various SAs with different working mechanisms have been introduced and widely applied, such as nonlinear polarization rotation (NPR) [2, 3], nonlinear optical loop mirrors (NOLMs) and nonlinear amplifying loop mirrors (NALMs) [4, 5], semiconductor saturable absorption mirrors (SESAMs) [6], and two-dimensional (2D) layered materials [7–9] (e.g. carbon nanotube, graphene, topological insulators, black phosphorus). However, NPR, and the NOLM and NALM are highly sensitive to environ-

mental perturbations (e.g. bending or twisting of the fiber in the cavity) and it is difficult to maintain good long-term stability. On the other hand, SESAM and 2D materials involve very complex and expensive fabrication processes and are subject to their narrow operation bandwidth, low damage threshold and complex packaging [10, 11]. These drawbacks make them impractical for certain applications and restrict their further development in high-power mode-locked lasers. Therefore, it is very important both to improve the performance of existing SAs and to develop new types of SAs to overcome these limitations.

Very recently, nonlinear multimodal interference (NL-MMI) in a graded index multimode fiber (GIMMF) has resulted in an effective saturable absorption effect and was successfully applied in various passively MLFLs [12–18]. These all-fiber SAs have the inherent advantages of a high damage threshold, wavelength independent operation, simple fabrication process and long-term stability which make them attractive for passive mode lockers operating in the high-power regime. A single mode fiber – graded index multimode fiber – single mode fiber (SMF-GIMMF-SMF) structure, Fig. 1(a), has been introduced as a simple SA, and several modified structures have been reported to improve the performance of the MMI SA. For example, by introducing a short segment of step-index MMF or an inner micro-cavity between the input SMF and GIMMF [19, 20], the relative power distribution of guided modes in the GIMMF was adjusted and the overall NL-MMI performance was improved by the enhanced higher-order mode content. However, fabrication of these segments is difficult, requiring careful arc control in fiber fusion splicing to form a micro-cavity in a fiber and/or particular bending or twisting to adjust the input launch condition, which leads to poor stability and reproducibility and makes these devices difficult to be apply in practice.

In this paper, we propose a simple but new reliable NL-MMI structure with a small-core fiber (SCF) as depicted in Fig. 1(b). A short length of SCF is spliced between input SMF and GIMMF in a SMF-GIMMF-SMF structure in order to enhance coupling of power into higher-order modes in the GIMMF and to enhance the nonlinear multimode interaction. First, we simulate

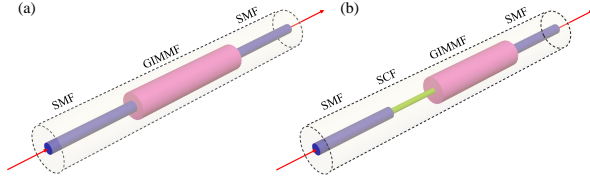


Fig. 1. Schematic of nonlinear multimode interference (NL-MMI) structures: (a) traditional SMF-GIMMF-SMF and (b) our proposed SCF-GIMMF-SMF.

the nonlinear pulse propagation along the GIMMF and identify the effectiveness of our proposed structure in terms of the modulation depth. Secondly, we experimentally measure the modulation depth of the device and evaluate the modal power distribution in a GIMMF using a time-of-flight measurement. Finally, we construct a passively mode-locked fiber ring laser using a SCF-GIMMF-SMF structure as an effective SA. Stable fundamental mode-locking operation was obtained at 1557.96 nm with a 647 fs pulse duration and a repetition rate of 19.37 MHz.

2. WORKING PRINCIPLE AND NUMERICAL SIMULATION

In a typical SMF-GIMMF-SMF structure, the fundamental mode of an input SMF is coupled to a superposition of guided modes in a GIMMF and recoupled back into the output SMF at a certain distance as a result of constructive multimode interference (MMI), called the “self-imaging” effect. All the guided modes in a GIMMF have nearly identical group velocities (i.e. minimal modal walk-off) and thus strong nonlinear intermodal interaction is expected among the guided modes in a GIMMF. The self-imaging condition can be expressed as [16]:

$$\beta_1 L_s + q2\pi = \beta_n L_s \quad (1)$$

where β_1 and β_n are the propagation constants of the fundamental mode and the n th guided mode of the GIMMF, respectively. q is an integer and L_s is the self-imaging distance with one oscillation period. In intra-cavity fiber lasers, the optical power is high enough to cause nonlinear phase shifts by self-phase modulation (SPM) and cross-phase modulation (XPM) effects in the GIMMF [16]. Therefore, the self-imaging condition in (1) can be rewritten as follows:

$$\beta_1 L'_s + q2\pi + (\gamma_1 P_1 + \gamma_{1n} P_n) L'_s = \beta_n L'_s + (\gamma_n P_n + \gamma_{1n} P_1) L'_s \quad (2)$$

where L'_s is the self-imaging distance shifted by nonlinear effects. γ_1 and γ_n are the nonlinear SPM coefficients for the fundamental mode and the n th mode, respectively. γ_{1n} is the coefficient for XPM, and P_1 and P_n are the optical powers in the fundamental mode and the n th mode, respectively. Combining (1) and (2), we can have

$$L'_s = \frac{\beta_1 - \beta_n}{(\beta_1 - \beta_n) + (\gamma_1 P_1 - \gamma_n P_n + \gamma_{1n} (P_n - P_1))} L_s \quad (3)$$

From Eq. (3), we noted that the self-imaging distance of a high-power signal is shorter than that of a low-power signal, which induces intensity-dependent transmission over a fixed GIMMF length. In other words, for a properly chosen GIMMF length a high-power signal has a higher transmission ratio than a low-power signal, which makes this SMF-GIMMF-SMF structure act as an effective SA. At the same time, the low mode

dispersion of the GIMMFs ensures that pulses do not break up in a short GIMMF segment.

We first performed numerical simulations to investigate the nonlinear optical pulse propagation in a GIMMF and the modulation depth of the proposed MMI structure. The numerical model uses the multimode nonlinear Schrödinger equation (NLSE) to solve short pulse propagation in a GIMMF [21]. The input pulse has a central wavelength of 1550 nm with a full-width half-maximum of 1 ps and an optical peak power is changed from 1 kW to 70 kW to investigate power dependent transmission. The fiber parameters were chosen according to our experiment (see Sec. 3): a commercial OM4 multimode fiber was used as a GIMMF (core diameter = 50 μ m, NA = 0.24) and an ultra-high NA SMF was employed as a SCF (core diameter = 2.2 μ m, NA = 0.35). This yields power coupling efficiencies from a SMF28 to the GIMMF LP₀₁ to LP₀₅ modes of 0.8305, 0.1406, 0.0238, 0.0040, 0.0007, respectively. Thus, 83% of the power is in the fundamental mode, which limits the achievable MMI. For the SCF, the coupling efficiencies are 0.2353, 0.1798, 0.1374, 0.1050, 0.0800, respectively. Hence, light is coupled efficiently into higher order modes and we can expect much stronger MMI.

We have calculated the transmission ratio of both MMI structures (i.e. SMF-GIMMI-SMF and SCF-GIMMI-SMF) along the propagation distance at different pulse peak powers and the simulation results are shown in Fig. 2. The transmission through the MMI structure shows a periodic power oscillation along the propagation distance due to the self-imaging effect. The nonlinear phase shifts change the self-focusing length in the GIMMF. As shown in Figs. 2(a) and 2(b), the self-focusing position shifts to the left as the pulse peak power increases in both MMI structures. **The shape of the transmission spectrum is defined by the superposition of guided modes in a GIMMF. In a SCF-GIMMF-SMF structure (Fig. 2b), the light is coupled efficiently into higher order modes and the transmission spectrum becomes less sinusoidal (or more complex) than that of SMF-GIMMF-SMF (Fig. 2a). However, the self-imaging distance, as calculated in equations (1)-(3), is affected by the effective refractive index difference (or group velocity difference) between the guided modes in a GIMMF and it is almost identical between two structures.**

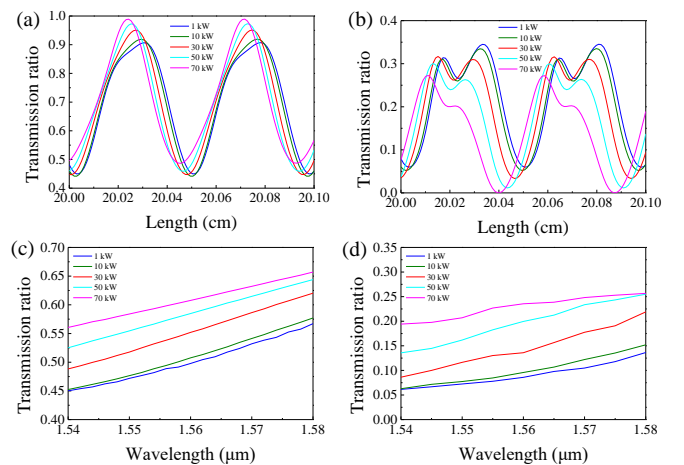


Fig. 2. Simulation results of both MMI structures. Transmission ratio of (a) SMF-GIMMF-SMF structure and (b) SCF-GIMMF-SMF structure along the propagation distance at different pulse peak powers at 1550 nm. Modulation depth of (c) SMF-GIMMF-SMF and (d) SCF-GIMMF-SMF structures when the length of the GIMMF is 20.006 cm.

Note that the higher the optical power, the higher the transmittance at a certain distance. Assuming an experimentally convenient fiber length of around 20 cm, the optimum GIMMF length of SMF-GIMMF-SMF and SCF-GIMMF-SMF structures is 20.006 cm according to our simulations. Figures 2(c) and 2(d) show the nonlinear transmission spectra for each structure over the wavelength range from 1540 nm to 1560 nm at the optimum GIMMF length. We see that for the SMF-GIMMF-SMF, transmission increases from 0.50 to 0.61 at 1560 nm, i.e., a 22% change for larger power. For the SCF-GIMMF-SMF, transmission increases from 0.09 to 0.24, an increase by a factor 2.7. Thus, while the SCF-GIMMF-SMF structure has larger intrinsic losses, its performance as a SA is significantly improved.

3. OPTICAL CHARACTERIZATION OF NONLINEAR MMI STRUCTURE

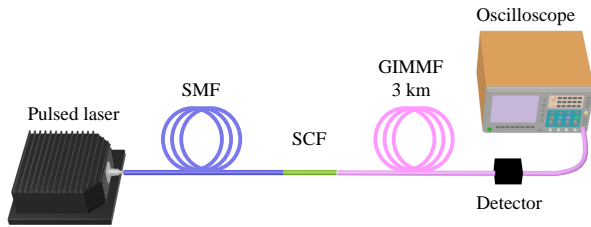


Fig. 3. Schematic of the experimental setup to measure the modal power distribution in a GIMMF.

To characterize the optical properties of the proposed structure, the modal power distribution in a GIMMF was measured using a time-of-flight method [22] and the experimental setup is shown in Fig. 3. A picosecond pulsed laser at 1552 nm was used as an input pulse source and the impulse response was measured at the end of fiber with a fast detector and an oscilloscope (Tektronix DSA8200). As each mode of interest possesses a distinct group velocity in the fiber, we can distinguish different spatial modes by their differential group delays (DGDs) and identify their relative power distribution. A 3 km length of additional GIMMF was spliced after the device to provide enough intermodal dispersion. In the SMF-GIMMF structure (Fig. 4(a)), most of the light is in the LP_{01} mode and the total power of the higher-order modes is less than 10%. However, in the SCF-GIMMF structure (Fig. 4(b)), many more higher-order modes can be excited in the GIMMF and the total power of the higher-order modes is 70%, which is beneficial for improving the NL-MMI modulation depth. Note that the input SMF/SCF is centrally aligned/spliced to the GIMMF and therefore only the circular symmetric LP_{0m} modes are excited in the GIMMF. The SCF, having a small mode field diameter ($\sim 4.0 \mu\text{m}$ at 1550 nm), effectively excites higher-order modes in the GIMMF because of the enhanced mode overlap with the LP_{0m} modes which have their peak intensity located at the fiber center.

As mentioned in the previous simulation in Fig. 2(b), there is an optimum GIMMF length to achieve the best modulation depth from our MMI structure and accurate fiber length control is very important. Typically, an accuracy of a few micrometers is required for the fiber length, which is difficult to achieve using conventional fiber cleaving or polishing techniques. In our experiment, therefore, we employ a fiber tension approach [15]. Approximately 20 cm of GIMMF is prepared and an axial tension is applied to the GIMMF to precisely control the effective fiber

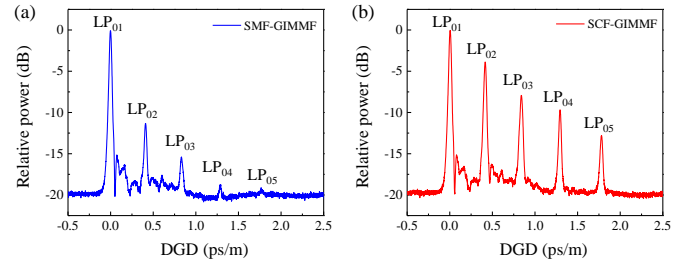


Fig. 4. Measured modal power distribution in a GIMMF for both (a) SMF-GIMMF and (b) SCF-GIMMF structure. DGD: differential group delay.

length. The stretched MMI SA is then connected to a commercial high-peak power fiber laser and the modulation depth was measured using a two-arm measurement method [16]. Figure 5 shows the measured modulation depth of our SCF-GIMMF-SMF structure at various pulse intensities. Here the dots are experimental data and the red line is a nonlinear fit with a saturable absorption curve given by $T(I) = 1 - \alpha \times \exp(-I/I_{sat}) - \alpha_{ns}$ [15], where T is the transmission, α is the modulation depth, I is the input light intensity, I_{sat} is the saturation intensity, and α_{ns} is the nonsaturable loss. Due to the peak power limitation of our available laser, we measured powers up to 2 kW but a modulation depth of 9% is expected from the fit at higher power level ($> 20 \text{ kW}$). The insertion loss of the proposed SCF-GIMMF-SMF structure was measured to be $\sim 4 \text{ dB}$.

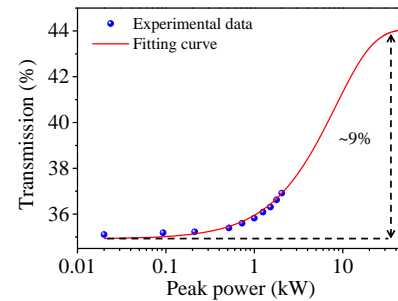


Fig. 5. Measured modulation depth of SCF-GIMMF-SMF structure. Blue dots are experimental data, red line is fitting curve.

4. PASSIVELY MODE-LOCKED FIBER LASER WITH A NONLINEAR MMI STRUCTURE

To verify the effectiveness of the proposed MMI structure, we constructed a passively MLFL with a SCF-GIMMF-SMF structure, as depicted in Fig. 6. A 1.5 m length of erbium-doped fiber (Er-30, Thorlabs) with group velocity dispersion (GVD) of $14.45 \text{ ps}^2/\text{km}$ was used as a gain medium and a 976 nm pump laser was coupled through a 980/1550 nm wavelength division multiplexing (WDM) coupler. 10% of the optical power was extracted from the laser cavity using a 10/90 tap coupler. The stretched SCF-GIMMF-SMF structure was included directly after the coupler and a polarization controller (PC) was used to adjust the polarization state of the laser cavity. SPM and XPM (on which our SA relies) depend on polarization, so polarization control is needed to maximise the effect. The total cavity length is 9.7 m and the net cavity dispersion of the laser is about -0.147 ps^2 , which results in a soliton operation. To avoid the NPR effect

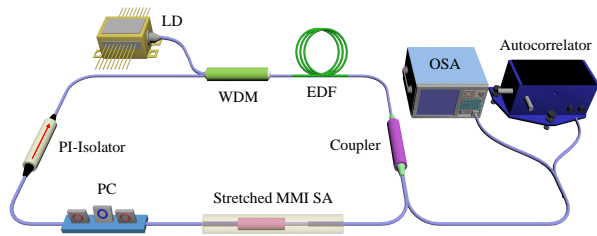


Fig. 6. Schematic of the mode-locked fiber laser with a NL-MMI structure. LD: laser diode; WDM: wavelength division multiplexing coupler; EDF: erbium-doped fiber; PC: polarization controller; PI-Isolator: polarization-independent isolator; OSA: optical spectrum analyzer.

and to enforce unidirectional laser operation, a polarization-independent isolator was inserted in the laser cavity. The output beam was recorded by an optical spectrum analyzer (OSA), an oscilloscope and an autocorrelator.

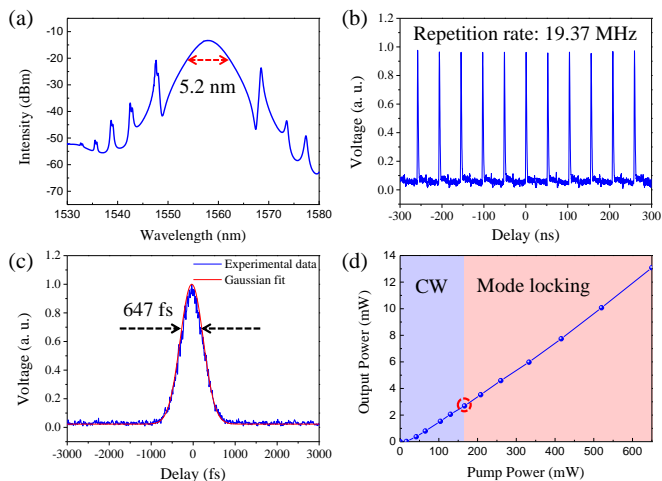


Fig. 7. Experimental results of the mode-locked fiber laser using the proposed SA. (a) Optical spectrum, (b) pulse train, (c) autocorrelation trace of the pulse, and (d) the power relationship between the pump power and output power. CW: continuous wave.

The mode-locked pulses are obtained by adjusting the tension of the MMI structure and the PC in the laser cavity. The pump threshold of the mode-locked operation was found at 166 mW and stable self-starting mode-locking was observed at higher powers. The pulse characteristics were recorded and analyzed when the fiber laser was operating in the mode-locked regime at a pump power of 416 mW. The output spectrum is shown in Fig. 7(a) and the signal to noise ratio is more than 40 dB. The output spectrum exhibits Kelly sidebands (typical for solitons in anomalous dispersion fiber lasers) and the 3-dB spectral bandwidth of the generated pulse was 5.2 nm at the central wavelength of 1557.96 nm. Figure 7(b) presents a typical pulse train in the time domain showing a repetition rate of 19.37 MHz and Fig. 7(c) shows the autocorrelation measurement of the pulse. The measured 3-dB pulse duration obtained by a Gaussian fit was ~ 647 fs. In Fig. 7(d), the average output power of the mode-locked soliton laser is shown as a function of pump power. Note that for pump powers below 166 mW the laser is operating in the continuous wave (CW) regime; mode-locking is

achieved by increasing the pump power again. The maximum output power at single pulse operation is measured to be 13 mW, corresponding to a pulse energy of 0.67 nJ (corresponding peak power ~ 1 kW). Note that this peak power is for the 10% output coupling and the peak power inside the laser cavity (i.e. relevant for the SA) should be 10 times higher (i.e. 10 kW), which is in line with the higher modulation depth on the right of Fig. 5. The output power was stable and repeatable in the laboratory environment and it was preserved for periods in excess of 1 hour (only small power fluctuation of $\sim 1.28\%$ peak-to-valley).

The output performance of our laser is compared to that of mode-locking operation using other NL-MMI based SAs in terms of central wavelength (λ_c), 3-dB bandwidth ($\Delta\lambda$), modulation depth (α), pulse duration ($\Delta\tau$), and output power (P_{out}) and are summarized in Table 1. It can be clearly seen that the proposed NL-MMI SA has a deeper modulation depth, wider working bandwidth and better P_{in}/P_{out} ratio, which makes the pulse duration narrower and more stable. This comparison strongly suggests that the proposed NL-MMI SA is highly comparable to previous reports and it can be used as a reliable all-fiberized mode-locking device for high power or high pulse energy fiber laser applications.

Table 1. Comparison of MLFLs with NL-MMI based SAs

Method	λ_c [nm]	$\Delta\lambda$ [nm]	α [%]	$\Delta\tau$ [fs]	P_{in}/P_{out} [mW]	Ref.
SIMMF ^a	1598	3.4	~ 2.75	960	700/24	[13]
GIMMF	1572.5	4.7	10.37	506	$\sim 210/1.8$	[15]
SIMMF	1596.66	2.18	~ 5	625	227/7.07	[16]
GIMMF	1063.42	0.62	~ 10	~ 350000	–	[17]
GIMMF	~ 1979	4.7	~ 1.5	–	300/2.7	[18]
SIMMF	1888	3.6	–	~ 1400	$\sim 900/9$	[19]
Microcavity	1558	4.14	~ 1.5	528	260/1.3	[20]
SIMMF	1560.9	4.48	~ 3.16	446	67.4/0.15	[23]
GIMMF	1931	3.77	9.5	~ 1200	110/0.25	[24]
SCF	1557.96	5.2	~ 9	647	650/13	This work

^a SIMMF: Step-index MMF.

5. CONCLUSION

In conclusion, we have proposed and demonstrated a stable SA based on an all-fiber NL-MMI structure suitable for high-power MLFL applications. Compared to previously reported SMF-GIMMF-SMF structures, the proposed SCF-GIMMF-SMF structure can provide larger modulation depth due to enhanced higher-order mode contributions in the multimode fiber. A $\sim 9\%$ modulation depth was experimentally estimated and a stable MLFL was demonstrated with a pulse width of 647 fs at a repetition rate of 19.37 MHz. The proposed all-fiber SA has multiple advantages such as high damage threshold, simple fabrication, low cost, and good stability and provides a highly promising route towards high-power fiber laser applications.

Funding. Engineering and Physical Sciences Research Council (EP/N00762X/1, EP/P030181/1); National Natural Science Foundation of China (NSFC) (91750108).

Acknowledgments. Xianglong Zeng acknowledges the Program for Professor of Special Appointment (Eastern Scholar) at Shanghai Institutions of Higher Learning. Teng Wang thanks the China Scholarship Council (CSC) for financial support.

282 **Disclosures.** The authors declare no conflicts of interest.

283 **Data availability.** Data underlying the results presented in this paper
284 are not publicly available at this time but may be obtained from the
285 authors upon reasonable request.

286 6. REFERENCES

287 REFERENCES

- 288 1. M. E. Fermann and I. Hartl, "Ultrafast fibre lasers," *Nat. Photonics* **7**,
289 868 (2013).
- 290 2. T. Wang, F. Wang, F. Shi, F. Pang, S. Huang, T. Wang, and X. Zeng,
291 "Generation of femtosecond optical vortex beams in all-fiber mode-
292 locked fiber laser using mode selective coupler," *J. Light. Technol.* **35**,
293 2161–2166 (2017).
- 294 3. T. Wang, A. Yang, F. Shi, Y. Huang, J. Wen, and X. Zeng, "High-order
295 mode lasing in all-FMF laser cavities," *Photonics Res.* **7**, 42–49 (2019).
- 296 4. F. Ilday, F. Wise, and T. Sosnowski, "High-energy femtosecond
297 stretched-pulse fiber laser with a nonlinear optical loop mirror," *Opt.*
298 *Lett.* **27**, 1531–1533 (2002).
- 299 5. M. A. Chernysheva, A. A. Krylov, P. G. Kryukov, and E. M. Dianov,
300 "Nonlinear amplifying loop-mirror-based mode-locked thulium-doped
301 fiber laser," *IEEE Photonics Technol. Lett.* **24**, 1254–1256 (2012).
- 302 6. O. Okhotnikov, T. Jouhti, J. Kontinen, S. Karirinne, and M. Pessa,
303 "1.5- μm monolithic gainnas semiconductor saturable-absorber mode
304 locking of an erbium fiber laser," *Opt. Lett.* **28**, 364–366 (2003).
- 305 7. B. Guo, Q. Xiao, S. Wang, and H. Zhang, "2D layered materials: syn-
306 thesis, nonlinear optical properties, and device applications," *Laser &*
307 *Photonics Rev.* **13**, 1800327 (2019).
- 308 8. G. Sobon, "Mode-locking of fiber lasers using novel two-dimensional
309 nanomaterials: graphene and topological insulators," *Photonics Res.* **3**,
310 A56–A63 (2015).
- 311 9. C. Ma, C. Wang, B. Gao, J. Adams, G. Wu, and H. Zhang, "Recent
312 progress in ultrafast lasers based on 2D materials as a saturable
313 absorber," *Appl. Phys. Rev.* **6**, 041304 (2019).
- 314 10. P. Yan, H. Chen, J. Yin, Z. Xu, J. Li, Z. Jiang, W. Zhang, J. Wang, I. L.
315 Li, Z. Sun *et al.*, "Large-area tungsten disulfide for ultrafast photonics,"
316 *Nanoscale* **9**, 1871–1877 (2017).
- 317 11. J. Yin, F. Zhu, J. Lai, H. Chen, M. Zhang, J. Zhang, J. Wang, T. He,
318 B. Zhang, J. Yuan *et al.*, "Hafnium sulfide nanosheets for ultrafast
319 photonic device," *Adv. Opt. Mater.* **7**, 1801303 (2019).
- 320 12. E. Nazemosadat and A. Mafi, "Nonlinear multimodal interference and
321 saturable absorption using a short graded-index multimode optical
322 fiber," *J. Opt. Soc. Am. B* **30**, 1357–1367 (2013).
- 323 13. F. Zhao, Y. Wang, H. Wang, X. Hu, W. Zhang, T. Zhang, and
324 Y. Cai, "High-energy solitons generation with a nonlinear multimode
325 interference-based saturable absorber," *Laser Phys.* **28**, 085104
326 (2018).
- 327 14. G. Chen, W. Li, G. Wang, W. Zhang, C. Zeng, and W. Zhao, "Generation
328 of coexisting high-energy pulses in a mode-locked all-fiber laser with a
329 nonlinear multimodal interference technique," *Photonics Res.* **7**, 187–
330 192 (2019).
- 331 15. Z. Wang, D. N. Wang, F. Yang, L. Li, C. Zhao, B. Xu, S. Jin, S. Cao,
332 and Z. Fang, "Stretched graded-index multimode optical fiber as a
333 saturable absorber for erbium-doped fiber laser mode locking," *Opt.*
334 *Lett.* **43**, 2078–2081 (2018).
- 335 16. T. Chen, Q. Zhang, Y. Zhang, X. Li, H. Zhang, and W. Xia, "All-fiber
336 passively mode-locked laser using nonlinear multimode interference of
337 step-index multimode fiber," *Photonics Res.* **6**, 1033–1039 (2018).
- 338 17. Z. Dong, J. Lin, H. Li, S. Li, R. Tao, C. Gu, P. Yao, and L. Xu, "Generation
339 of mode-locked square-shaped and chair-like pulse based on reverse
340 saturable absorption effect of nonlinear multimode interference," *Opt.*
341 *Express* **27**, 27610–27617 (2019).
- 342 18. K. Zhao, Y. Li, X. Xiao, and C. Yang, "Nonlinear multimode interference-
343 based dual-color mode-locked fiber laser," *Opt. Lett.* **45**, 1655–1658
344 (2020).
- 345 19. H. Li, Z. Wang, C. Li, J. Zhang, and S. Xu, "Mode-locked Tm fiber laser
346 using SMF-SIMF-GIMF-SMF fiber structure as a saturable absorber,"
347 *Opt. Express* **25**, 26546–26553 (2017).
- 348 20. F. Yang, D. Wang, Z. Wang, L. Li, C. Zhao, B. Xu, S. Jin, S. Cao, and
349 Z. Fang, "Saturable absorber based on a single mode fiber-graded
350 index fiber-single mode fiber structure with inner micro-cavity," *Opt.*
351 *Express* **26**, 927–934 (2018).
- 352 21. F. Poletti and P. Horak, "Description of ultrashort pulse propagation in
353 multimode optical fibers," *J. Opt. Soc. Am. B* **25**, 1645–1654 (2008).
- 354 22. J. Cheng, M. E. Pedersen, K. Wang, C. Xu, L. Grüner-Nielsen, and
355 D. Jakobsen, "Time-domain multimode dispersion measurement in a
356 higher-order-mode fiber," *Opt. Lett.* **37**, 347–349 (2012).
- 357 23. Z. Wang, D. Wang, F. Yang, L. Li, C. Zhao, B. Xu, S. Jin, S. Cao, and
358 Z. Fang, "Er-doped mode-locked fiber laser with a hybrid structure of a
359 step-index-graded-index multimode fiber as the saturable absorber," *J.*
360 *Light. Technol.* **35**, 5280–5285 (2017).
- 361 24. H. Li, F. Hu, Y. Tian, P. Wang, J. Zhang, and S. Xu, "Continuously
362 wavelength-tunable mode-locked Tm fiber laser using stretched SMF-
363 GIMF-SMF structure as both saturable absorber and filter," *Opt. Ex-*
364 *press* **27**, 14437–14446 (2019).